A Feasibility Study on the Position Hypothesis Based RTK with the Aids of 3D Building Models

Hoi-Fung Ng, *Interdisciplinary Division of Aeronautical and Aviation Engineering, The Hong Kong Polytechnic University*
Li-Ta Hsu, *Interdisciplinary Division of Aeronautical and Aviation Engineering, The Hong Kong Polytechnic University*

BIOGRAPHY (IES)

Hoi-Fung NG received a Bachelor of Engineering (Honours) in Air Transport Engineering from The Hong Kong Polytechnic University, Hong Kong, in 2018.
He is currently an M.Sc. student at the Department of Mechanical Engineering, The Hong Kong Polytechnic University, Hong Kong. His research interests including GNSS localisation, navigation.

Li-Ta HSU received the B.S. and Ph.D. degrees in aeronautics and astronautics from National Cheng Kung University, Taiwan, in 2007 and 2013, respectively. He is currently an assistant professor with the Division of Aeronautical and Aviation Engineering, Hong Kong Polytechnic University, before he served as post-doctoral researcher in Institute of Industrial Science at University of Tokyo, Japan. In 2012, he was a visiting scholar in University College London, U.K. He is an Associate Fellow of RIN. His research interests include GNSS positioning in challenging environments and localisation for pedestrian, autonomous driving vehicle and unmanned aerial vehicle.

ABSTRACT

High precision positioning has become the point of discussion for many revolutionary applications. Like unmanned autonomous system (UAS), requires a highly precise positioning with centimeter-level accuracies. Real-time Kinematic (RTK) is one of the most precise positioning technologies and provide a centimeter-level positioning in opensky or sub-urban environment. However, in the urban environment, severe non-line-of-sight (NLOS) and multipath effects degrade the RTK GNSS positioning. Ambiguity resolution (AR) is the key for RTK GNSS, the carrierphase measurement with integer ambiguity resolved can provide a centimeter accuracy for positioning. The NLOS reception and multipath effect mentioned will result in a noisy measurement for AR and result in low fixing rate in the urban area for RTK GNSS. Therefore, removal on the bad measurements and remain those good-condition signal become essential for RTK GNSS. We believed that NLOS satellite exclusion by 3D building model dynamically is better comparing to with fixed elevation angle. Based on this idea, the study proposes using the 3D building model with position hypothesis to filter out unhealthy satellite from AR and RTK positioning, namely 3DMA GNSS RTK. The designed experiment in Hong Kong urban environment with geodetic-grade receivers will be used to evaluate the performance of our proposed algorithm. The experiment results show that 3DMA GNSS RTK can provide positioning accuracy with 10cm averagely.

INTRODUCTION

Accurate global navigation satellite system (GNSS) positioning with high accuracy is important for different location-based service (LBS) application, especially unmanned autonomous system (UAS) requires centimeter-level accuracies. However, the urban canyon is always a challenge for GNSS to achieve good position results as the GNSS signal can be blocked or reflected by the buildings, which are non-line-of-sight (NLOS) reception and multipath (MP) effect [1]. These effects will create a large positioning error [2]. In ranging-based positioning, using 3D building model is one of the popular methods to mitigate the effects on MP and NLOS in urban positioning, which is 3D mapping aided (3MDA) GNSS [3]. 3D building model can use to detect and exclude the NLOS signal for the positioning [4]. Our previous works included the ray-tracing 3DMA GNSS [5, 6] and skymask 3DMA GNSS [7] predict the signal path and correct the NLOS reception pseudorange. The integration solution on the shadow matching likelihood-based 3DMA GNSS, and skymask 3DMA GNSS to improve both along and across street accuracy was introduced [8]. The integrated solution can provide about 5m to 10m accuracies in urban areas [9].

The ranging-based positioning can provide a performance of several meters currently, however, this is not enough for automotive applications. Especially the trend on the development of autonomous driving, centimeter-level positioning accuracy is essential for real use. Therefore, the real-time-kinematic (RTK) [10] stands an important role to provide highly accurate positioning. The RTK integrates the code measurements with the carrierphase measurements to provide a centimeter accuracy positioning. The measurements are first double-differenced between the base station & rover and master & slave satellites. Then the least-square approach is used to obtain the float solution of rover position and integer ambiguity. Then the integer ambiguity resolution (AR) by the LAMBDA [11] and ratio test are performed. If the ratio test is larger than the threshold, the solution will be the fix solution, named Integer Least-Squares (ILS) [11]. With multiple constellations and frequencies of measurements, the RTK GNSS fixed solution can obtain within 5cm error with about 95% fixed rate [12]. Another approach is weighted average all the integer sets to obtain the integer ambiguities, namely Best Integer Equivariant (BIE) [13]. The BIE performs integer-summation rather than one finite integer set, which can maintain the property of integer-equivariance. This is applicable for the situation that carrierphase measurements are noisy while the quality of ambiguity are not good enough to obtain a fixed solution, like a low-cost receiver located in an urban environment. [14] has demonstrated the BIE performance on a low-cost single-frequency GNSS receiver. Where BIE positioning accuracy is better than that of the float solution and better than ILS fixed solutions when success rate is low [15].

A sufficient number of healthy satellites is the key factor for RTK positioning. RTK always outperforms in opensky environments, and obtain a satisfactory performance in rural and suburban areas. However, in urban canyons, the performance of RTK cannot be maintained due to the NLOS and MP effects will produce unhealthy carrierphase measurements and degrade the performance. To achieve better performance of RTK positioning in urban environments, excluding the unhealthy measurements is one of the approaches. Research in [16] proposed a cycle slip detection scheme and fixed by the MEMS-IMU to perform the RTK positioning. In [17], implemented using the sky-pointing fisheye camera with image processing technique to exclude the NLOS received satellites where this approach is suitable for vehicle-mounted application such as autonomous driving.

Some other researches propose cooperating the 3D building model to aid the RTK positioning in the urban area, which no extra equipment is required, like the continuous-LOS method [18]. Assuming the signals can be tracked and received continuously, a better quality of the measurements are. Therefore, better positioning results can be obtained with only healthy code and carrierphase measurements. These researches show that selecting correct satellites for RTK is important. Also, [19] proved that with the 3D maps, RTK GNSS could be achieved when approximate positions were within 5-15m from the true position. For the UAS application, the 3D maps can help the path planning to avoid GNSS challenging places and maximize the performance of RTK GNSS [20].

To improve the performance of RTK in urban canyons, this study proposes to bring the 3DMA GNSS concept with a hypothesis-based approach into the RTK positioning. A conventional RTK GNSS is used as an initial position for the distribution of hypothesized-candidates. At each candidate, NLOS exclusion based on 3D models is performed. The survived satellites at each candidate are used for AR and modelling the ambiguities resolved carrierphase. The score is given to each candidate based on the difference between the modelled and observed carrierphase measurements. The smaller it is, the higher score will be given. By weighted (based on the score) averaging the location of the all hypothesized candidates, the ‘best float position’ is obtained. Noted that the ‘best float position’ does not mean it is a fixed position. The satellite visibility at ‘best float position’ is used for AR again to find the fixed solution as the 3DMA GNSS RTK solution.

The preliminary results are tested by the experiment in suburban and urban environments in Hong Kong with geodetic-grade receiver Novatel FlexPak6. The 3DMA GNSS RTK shows that it can improve the positioning accuracy compare to the conventional one, which the positioning results can achieve within 10cm with a geodetic grade receiver in the urban environments.

A reminder of the structure of the paper as we will briefly introduce the conventional RTK GNSS first, then present our proposed 3DMA GNSS RTK. After that, the designed experiments and their results will be presented.

THE PROPOSED 3DMA GNSS RTK

The flowchart of the proposed 3DMA GNSS RTK is shown in Figure 1. The algorithm can be divided into online and offline processes. The offline stage includes processing the 3D building model for NLOS classification. Here, we utilise the resource from GNSS shadow matching, which is the skyplot with highest elevation angle of the building boundaries, known as ‘skymask’ [7]. At the online stage, the real-time RTK positioning and 3DMA GNSS RTK are performed. First, the conventional RTK positioning with

ambiguity resolution is performed and used as an initial guess. Based on the RTK solution, the hypothesis positioning candidates can be distributed. On each candidate, the satellite visibility will be estimated, then find the float solution and follow by AR. The fixed ambiguity will be used to model the carrierphase based-on candidate and compare with received measurements, a score will be given to each candidate based on the consistency between modelled and observed carrierphase. Then a weighted average position can be found, and it is used as an accurate float solution for the 3DMA GNSS RTK. The float solution will then perform NLOS exclusion and ambiguity resolution by BIE-estimator again to find the fixed solution.

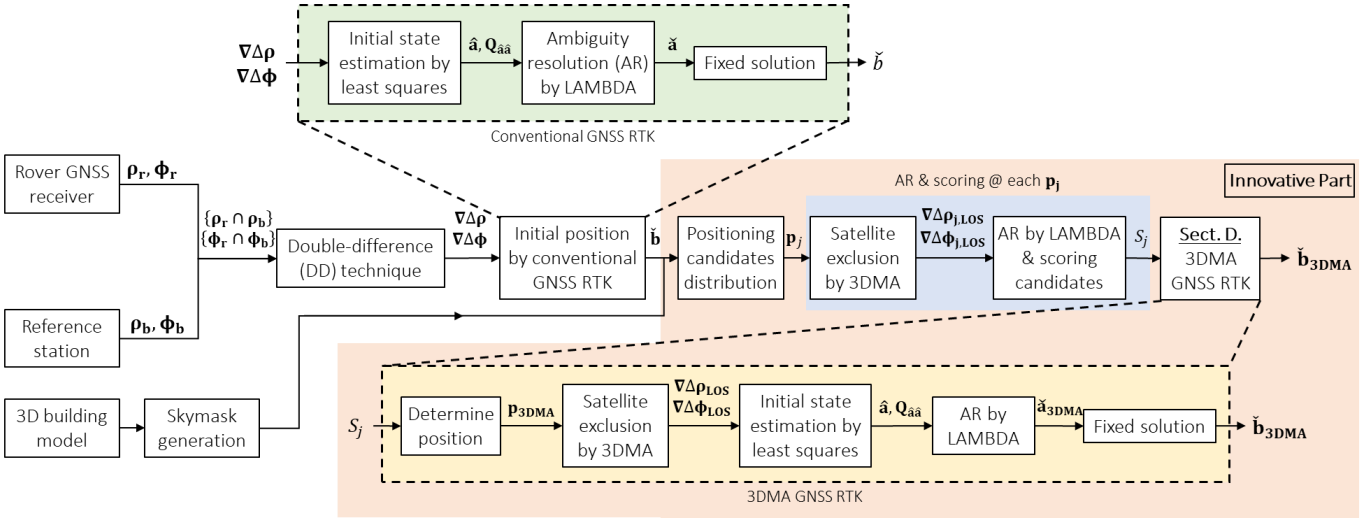

Figure 1 Flowchart of the proposed 3DMA GNSS RTK.

Conventional GNSS RTK and Ambiguity Resolution (AR)

GNSS RTK cooperates both code (pseudorange) and carrierphase measurements to resolve the rover (receiver) position by estimating the relative distance to a baseline reference station. In this paper, we use multi-constellation and dual-frequency measurements. All measurements will perform a simple selection with C/N_0 larger than 15dB-Hz and elevation angle el larger than 15-degrees. The implemented GNSS RTK is based on the [21].

The commonly received satellites by rover and base station are first double-differenced (DD). DD formulation is in system-specific pivot satellite manner, where one master satellite, $*^m$ for each constellation and measurement frequency. In theory, DD can eliminate the tropospheric error, satellite clock error, and receiver clock error. The DD term remains the double-differenced geometry distance and other error terms from receiver noise for both pseudorange and carrierphase measurements. The carrierphase measurements also have extra double differenced integer ambiguity term, where this will be resolved an integer value by AR later. The DD code $\nabla\Delta\rho$ and carrier $\nabla\Delta\phi$ measurements for the i-th and commonly received satellite at both rover SV_r and base station SV_b can be expressed in meter, as,

$$\begin{aligned}\nabla\Delta\rho^i &= \rho_r^i - \rho_r^m - \left(\rho_b^i - \rho_b^m\right) = \nabla\Delta D^i + \varepsilon_{\rho^i} \\ \nabla\Delta\phi^i &= \phi_r^i - \phi_r^m - \left(\phi_b^i - \phi_b^m\right) = \nabla\Delta D^i + \lambda^i\nabla\Delta N^i + \varepsilon_{\phi^i}\end{aligned} \tag{1}$$

where $*_r$ stands for rover data while $*_b$ stands for base station data. $\nabla\Delta D$ is the double-differenced geometry distance. ε_* is other error terms from receiver noise, etc. λ^i is the wavelength of the i-th common satellite between rover and base station (excluding the master one). $\nabla\Delta N$ is the double differenced integer ambiguity, where this will be obtained by AR. The DD geometric distance for satellite i to the receiver is calculated by the Pythagoras theorem of satellite ECEF position and receiver ECEF position,

$$D_*^i = \left\|\mathbf{p}^i - \mathbf{p}_*\right\| = \sqrt{\left(p_x^i - p_{*,x}\right)^2 + \left(p_y^i - p_{*,y}\right)^2 + \left(p_z^i - p_{*,z}\right)^2} \tag{2}$$

The geometric distance is applicable for both rover and reference station, D_r^i and D_b^i, respectively. Therefore, the DD of the geometric distance between receiver and satellite can be expressed as,

$$\nabla\Delta D^i = D_r^i - D_r^m - \left(D_b^i - D_b^m\right) \tag{3}$$

The initial state estimation on the float position and ambiguities is done by the least-squares (LS) method.

$$\hat{\mathbf{x}} = \mathbf{N}^{-1}\mathbf{A}^{\mathrm{T}}\mathbf{Q}^{-1}\boldsymbol{y} \tag{4}$$

where $\mathbf{N}$ is the normal matrix calculated by $\mathbf{N} = (\mathbf{A}^{\mathbf{T}}\mathbf{Q}^{-\mathbf{1}}\mathbf{A})$. $\mathbf{Q}$ is the cofactor matrix, which is formed by the weighting factor of each satellite and its pivot satellite. $\mathbf{A}$ is the design matrix of the baseline and ambiguities. The first three columns of the design matrix are the difference of the unit LOS vector for the satellites. While the upper right is a zero matrix and lower right is a diagonal matrix of wavelength for corresponding satellite. $\mathbf{y}$ is the measurement vector.

$$\mathbf{A} = \begin{bmatrix} \mathbf{u_r^1} - \mathbf{u_r^m} & 0 & \dots & 0 \\ \vdots & \vdots & \ddots & \vdots \\ \mathbf{u_r^i} - \mathbf{u_r^m} & 0 & \dots & 0 \\ \mathbf{u_r^1} - \mathbf{u_r^m} & \lambda^1 & \dots & 0 \\ \vdots & \vdots & \ddots & \vdots \\ \mathbf{u_r^i} - \mathbf{u_r^m} & 0 & \dots & \lambda^i \end{bmatrix} \text{ where } \mathbf{u_r^*} = \frac{\mathbf{p_r} - \mathbf{p}^*}{D_r^*} = \left[\frac{p_{r,x} - p_x^*}{D_r^*}, \frac{p_{r,y} - p_y^*}{D_r^*}, \frac{p_{r,z} - p_z^*}{D_r^*}\right] \tag{5}$$

$$\mathbf{y} = \begin{bmatrix} \nabla\Delta\rho^1 - \nabla\Delta D^1 \\ \vdots \\ \nabla\Delta\rho^i - \nabla\Delta D^i \\ \nabla\Delta\phi^1 - \nabla\Delta D^1 \\ \vdots \\ \nabla\Delta\phi^i - \nabla\Delta D^i \end{bmatrix} \tag{6}$$

The LS estimated float solution constructed by two main parts, first is the baseline between the rover and reference station to compute the float position in ECEF coordinates $\hat{\mathbf{b}}$, and the second part is the float DD ambiguities $\hat{\mathbf{a}}$.

$$\mathbf{x} = \left[b_x, b_y, b_z, \nabla\Delta N^1, \dots, \nabla\Delta N^i\right]^{\mathrm{T}} \tag{7}$$

Then the normalized weighted sum of the squared measurement residuals of the LS can be obtained. Therefore, the ambiguity variance-covariance (VC) matrix $\mathbf{Q}_{\hat{\mathbf{a}}\hat{\mathbf{a}}}$ can be found. The float DD ambiguities $\hat{\mathbf{a}}$ and ambiguity VC matrix $\mathbf{Q}_{\hat{\mathbf{a}}\hat{\mathbf{a}}}$ will input to LAMBDA and resolve an integer ambiguity. The main goal of ambiguity resolution (AR) is to find an integer vector that can minimize the squared error of LS estimated float ambiguity vector $\hat{\mathbf{a}}$, given that,

$$\min_{\mathbf{a}} \|\hat{\mathbf{a}} - \mathbf{a}\|^2_{\mathbf{Q}^{-1}_{\hat{\mathbf{a}}\hat{\mathbf{a}}}} \text{ where } \mathbf{a} \in \mathrm{Z}^n \tag{8}$$

The integer set with minimal squared error will be the fixed integer set for ILS. In this study, the BIE-estimator will also be used to obtain the ambiguity set $\bar{\mathbf{a}}$ for RTK solution. As we believed that the success rate is low to obtain a fixed solution in the urban area for ILS. Where BIE positioning accuracy is better than that of the float solution and better than ILS fixed solutions in this situation. Ambiguity set is calculated by the weighted average of the integer set found by LAMBDA [13]. The BIE baseline precision is always better than or as good as the precision of its float and fixed counterparts [18]. Which the positioning performance is similar to that of the ILS estimator and better than the float solution.

$$\bar{\mathbf{a}} = \sum_{\mathbf{a}\in\Theta^{\lambda}_{\hat{a}}} z \frac{\exp\left(-\frac{1}{2}\|\hat{\mathbf{a}}-\mathbf{a}\|^2_{\mathbf{Q}_{\hat{\mathbf{a}}\hat{\mathbf{a}}}}\right)}{\sum_{\mathbf{a}\in\Theta^{\lambda}_{\hat{\mathbf{a}}}} \exp\left(-\frac{1}{2}\|\hat{\mathbf{a}}-\mathbf{a}\|^2_{\mathbf{Q}_{\hat{\mathbf{a}}\hat{\mathbf{a}}}}\right)} \text{ with } \Theta^{\lambda}_{\hat{\mathrm{a}}} = \left\{\mathbf{a} \in \mathrm{Z}^n \mid \|\hat{\mathbf{a}} - \mathbf{a}\|^2_{\mathbf{Q}_{\hat{\mathbf{a}}\hat{\mathbf{a}}}} < \chi^2\right\} \tag{9}$$

BIE estimator obtains the ambiguity set by taking the integer-summation over finite integer set $\mathbf{a}$ inside n-dimension integer space Z^n by tuning the ellipsoidal region constant χ^2, where depends on the float solution and its variance matrix.

The BIE estimated ambiguity set $\bar{\mathbf{a}}$ is then used to calculate the fixed solution $\check{\mathbf{b}}$.

$$\check{\mathbf{b}} = \hat{\mathbf{b}} - \mathbf{Q}_{\hat{\mathbf{b}}\hat{\mathbf{a}}}\mathbf{Q}^{-\mathbf{1}}_{\hat{\mathbf{a}}\hat{\mathbf{a}}}(\hat{\mathbf{a}} - \bar{\mathbf{a}}) \tag{10}$$

where both BIE estimated ambiguity set $\bar{\mathbf{a}}$ and fixed solution $\check{\mathbf{b}}$ should be subjected to the minimization constrain.

Scoring at Positioning Hypothesis Candidate

Similar to the ranging-based, hypothesis candidate will be distributed around an initial position, the position solution of conventional GNSS RTK will be used here. Candidates will be scored based on the observed and the modelled measurements, the higher score candidate should be the position near the ground truth in theoretically [22]. 3DMA GNSS RTK will use the visibility at the weighted average position of the distributed candidate as the best set of the healthy satellite. On each candidate *j*, a score will be given based on matchness between the DD carrierphases $\nabla\Delta\boldsymbol{\phi}$ that survived from the skymask aided NLOS exclusion and the simulated DD carrierphases $\nabla\Delta\widetilde{\boldsymbol{\phi}}_j$ based on the position candidate *j*. The weighted average candidates based on the given score will be the 'accurate

float position' for visibility estimation. Noted that here we name it accurate float position as the ambiguities have not mapped to integer space and it is not the final solution for 3DMA GNSS RTK.

Similar to other 3DMA GNSS algorithm [9], hypothesis position candidates are distributed around the initial position by conventional GNSS RTK with 5m radius and 50cm resolution. Visibility and ambiguity will be estimated, and the score will be given to the candidate to represent the probability of a candidate being the ground truth or not. The ambiguity resolution is going to use BIE-estimator at each candidate due to its superiority under noisy measurement [14]. Identical to conventional GNSS RTK, healthy measurement with C/N_0 value larger than 15dB-Hz and elevation angle el larger than 15-degree will be selected. Also, at each candidate P_j, satellites will first perform LOS/NLOS classification with continuous-LOS estimation proposed in [18] to select healthy measurements. In each candidate, survived code and carrierphase measurements at candidate are first to double differenced as same as the conventional GNSS RTK, same as (1). Then, the survived DD measurements are used to LS and estimate the float ambiguities $\hat{\mathbf{a}}_j$ and its VC matrix $\mathbf{Q}_{\hat{\mathbf{a}}\hat{\mathbf{a}},\mathbf{j}}$ by (4)-(7). The integer ambiguity at candidate j will be resolved by the LAMBDA with BIE-estimator [13]. The BIE-estimator will be employed to find the weighted average of integer sets $\boldsymbol{z}$. For the ambiguities at j-th candidate, denoted as $\bar{\mathbf{a}}_j$, is then given as,

$$\bar{\mathbf{a}}_j = \sum_{\boldsymbol{z}\in\Theta} \boldsymbol{z} \frac{\exp\left(-\frac{1}{2}\|\hat{\mathbf{a}}_j-\boldsymbol{z}\|^2_{\mathbf{Q}_{\hat{\mathbf{a}}\hat{\mathbf{a}},j}}\right)}{\sum_{\boldsymbol{z}\in\Theta}\exp\left(-\frac{1}{2}\|\hat{\mathbf{a}}_j-\boldsymbol{z}\|^2_{\mathbf{Q}_{\hat{\mathbf{a}}\hat{\mathbf{a}},j}}\right)} \text{ with } \Theta = \left\{\boldsymbol{z}\in Z^n \mid \|\hat{\mathbf{a}}-\boldsymbol{z}\|^2_{\boldsymbol{Q}_{\hat{\boldsymbol{a}}\hat{\boldsymbol{a}},\boldsymbol{j}}} < \chi^2\right\} \tag{11}$$

After the integer ambiguity is resolved, we can obtain the score for the j-th candidate. By comparing the difference between measured and modelled DD carrierphase. The DD carrierphase mainly consists of the DD geometric distance and the DD integer ambiguities. Where DD geometric distance is calculated by (2) and (3), and the position is based on candidate ECEF position, e.g. $\mathbf{p}_* = \mathbf{p}_j$ in (2).

$$\nabla\Delta\tilde{\phi}^i_j = \nabla\Delta D^i_j + \lambda^{\mathrm{i}}\bar{a}^i_j \tag{12}$$

The score for the j-th candidate S_j can be obtained by the mean square error between measurements and modelled carrierphase based on the Gaussian noise assumption.

$$S_j = \exp\left[-0.5 \times \frac{1}{I}\sum_{i=1}^{I}\left(\nabla\Delta\phi^i - \nabla\Delta\tilde{\phi}^i_j\right)^2\right] \tag{13}$$

where I is the total number of survival satellites after exclusion at candidate j. Noted that in the $\left(\nabla\Delta\phi^i - \nabla\Delta\tilde{\phi}^i_j\right)$, if the candidate is closer to the ground truth, the value of $\nabla\Delta D^i_j$ will be close to the measurement $\nabla\Delta\phi^i$ itself. As a result, the better integer ambiguity $\bar{a}^i_j$ can be obtained to describe the carrierphase measurements $\nabla\Delta\phi^i$. In other words, a smaller value of $\left(\nabla\Delta\phi^i - \nabla\Delta\tilde{\phi}^i_j\right)$, as well as the mean square error (MSE) $\frac{1}{I}\sum_{i=1}^{I}\left(\nabla\Delta\phi^i - \nabla\Delta\tilde{\phi}^i_j\right)^2$, a higher score will be given.

After scoring each candidate, the accurate float position can be found by weighted averaging the candidate $\mathbf{p}_j$ with their score S_j, where there are total J positioning candidates.

$$\mathbf{p}_{3DMA} = \frac{\sum_{j=1}^{J} S_j \times \mathbf{p}_j}{\sum_{j=1}^{J} S_j} \tag{14}$$

$\mathbf{p}_{3DMA}$ plays a role in providing accurate float solution to the AR. At the accurate float position $\mathbf{p}_{3DMA}$, the AR with BIE-estimator will be done once again to refine the positioning result.

DESIGNED EXPERIMENT AND RESULTS

Several experiments were conducted in different suburban and urban canyons in Hong Kong and post-processed to evaluate the performance of 3DMA GNSS RTK. Measurements were collected using the geodetic grade NovAtel FlexPak6. L1- and L2-band frequencies are enabled for GPS (L1 and L2) and BeiDou (B1 and B2) during data collection. An active antenna was employed and connected to two receivers with a splitter to have a common-ground on signal receiving. We modified the open-source code goGNSS [23] to implement the proposed method in this paper for evaluation.

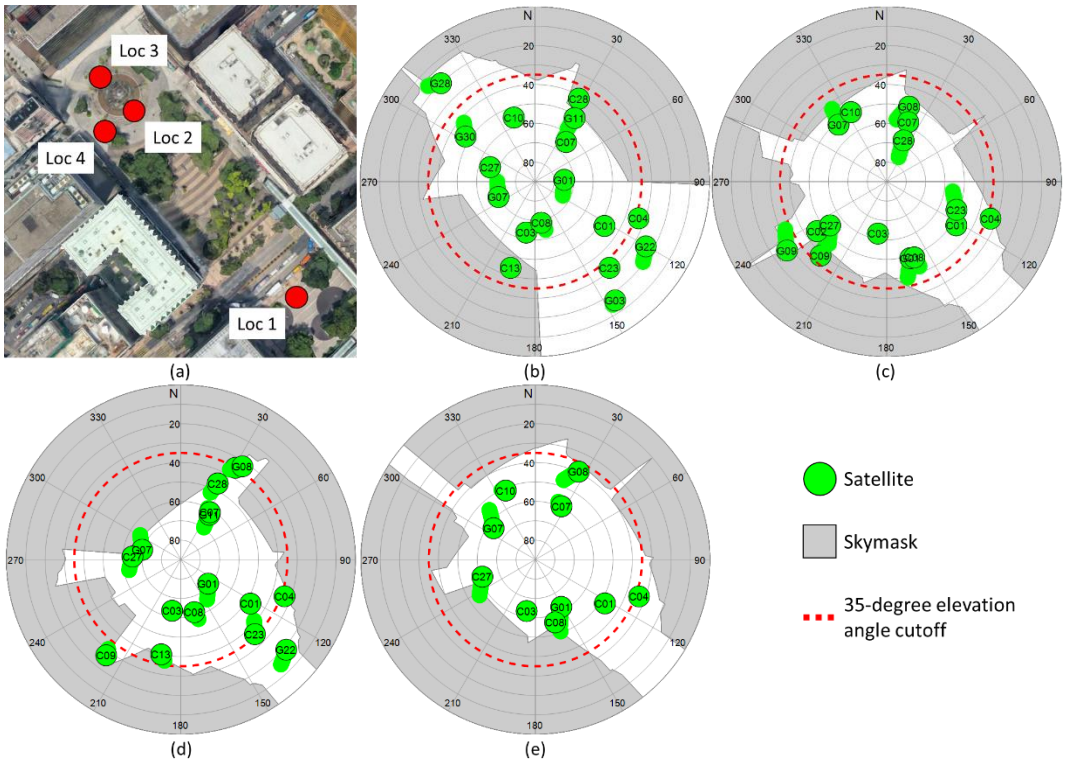

Figure 2 (a) Experiment location in Hong Kong urban areas. (b)-(e) Skymask at experiment location 1-4, respectively.

Table 1 Experiment information.

Location	Number of epochs (at 1Hz output rate)	Scenario	Skymask elevation angle mean (degree)	Skymask elevation angle STD (degree)	Skymask Maximum elevation angle (degree)
1	900	Suburban	30.6	21.0	55.9
2	1200	Urban	36.9	12.8	51.7
3	1200	Urban	43.2	17.9	67.6
4	900	Urban	37.8	15.7	58.3

Figure 3 Experiment equipment.

The positioning accuracy of this study is in centimetre-level, the determination of experiment ground truth is important here. When doing the experiment, the RTK estimated by NovAtel Flexpak 6 is performed at the meanwhile to get the average best position as the ground truth. Hong Kong Satellite Positioning Reference Station Network (SatRef) service by Hong Kong Land Department is employed for providing base station RTK message. Base station 'HKSC' is selected for the short baseline double differencing, where the geometric distance is about 4.6 km to the experiments' location averagely.

When conducting the experiment, before start recording the raw measurements, we wait until the NovAtel receiver to resolve the position type on narrow integer solution ('NARROW_INT' output), which is multi-frequency RTK solution with carrierphase ambiguities resolved to narrow-lane integers. After the narrow-lane solution are obtained about one-minute, we start to record the raw measurements for both receivers while the NovAtel keeps outputting the RTK solution at the same time. At the post-processing stage, all the resolved narrow-lane integers RTK solution will be extracted and taking average as the ground truth. Table 2 shows the error statistic on the difference between averaged ground truth and all narrow-lane output.

Table 2 Ground truth information estimated by NovAtel Flexpak 6. STD stands for standard deviation.

Experiment	No. of position output (at 1Hz)	Percentage of narrow-lane solution	Maximum 2D error (cm)	Minimum 2D error (cm)	Mean 2D error (cm)	STD of 2D error (cm)
1	967	97.6%	3.64	0.37	1.18	0.66
2	1321	99.6%	2.56	0.37	0.93	0.50
3	1005	99.4%	4.25	0.43	1.33	0.77
4	1292	80.0%	2.56	0.37	0.93	0.50

The average difference between calculated ground truth and all narrow-lane position is about 1cm with standard deviation (STD) about 0.5cm. The calculated position as ground truth should able to evaluate the RTK performance of different algorithms, however, if the positioning difference between two algorithms is within 1cm, it is hard to determine which algorithm performs better theoretically.

Positioning Results of Designed Experiments

The post-processed results will be summarized and compared with several positioning algorithms, including:

1. **ILS**
   Position with AR by LAMBDA method, without 3DMA exclusion.
2. **BIE**
   Position with AR by LAMBDA and BIE estimator, without 3DMA exclusion.
3. **BIE@EL35**
   The position with AR by BIE estimator, increase elevation angle cutoff to 35-degree. This method is selected because many of the existing works adopt high elevation angle mask assumption in urban GNSS RTK [24].
4. **3DMA BIE RTK**
   The position with AR by BIE estimator, and visibility estimation at accurate float position with 3DMA exclusion, which is the proposed method.
5. **3DMA BIE@GT (theoretically the best)**
   The position with AR by BIE estimator, visibility estimation at ground truth and 3DMA exclusion. This method is theoretically the best solution, as both the initial state and visibility are both estimated at ground truth.

The initial state estimation method, AR method, and other satellite selection parameters are shown in Table 3. The constant for continuous-LOS estimation is same as the value in [18]. Where GPS is set to 6s and BDS is set to 15s. And the first 6s will not exclude any satellite until the starting to exclude the GPS satellite.

Table 3 Post-processing information and parameters for different algorithms

Algorithm	Initial state estimation	AR method	Applying 3DMA	Applying continuous LOS (C-LOS)	Elevation cutoff angle (degree)	C/N_0 cutoff (dBHz)
ILS	Least square	LAMBDA	No	No	15	15
BIE	Least square	BIE	No	No	15	
BIE@EL35	Least square	BIE	No	No	35	
3DMA BIE RTK	Accurate float position	BIE	Yes	Yes	15	
3DMA BIE@GT	Ground truth	BIE	Yes	Yes	15	

The positioning results of NovAtel receiver on all experiment are summarized in Table 4. The 2D positioning error statistics are categorized in root-mean-square (RMS) error, and maximum (Max) error.

Table 4 Summary of 2D positioning results in experiment 1-5. (Unit: cm)

Experiment		ILS	BIE	BIE@EL35	3DMA BIE RTK	3DMA BIE@GT
1	RMS	391.36	382.83	306.86	7.47	7.47
	Max	1254.11	1157.70	885.38	203.68	203.68
2	RMS	0.90	0.90	0.95	0.93	0.95
	Max	2.09	2.09	1.97	2.09	2.09
3	RMS	257.25	241.76	30.11	7.95	8.11
	Max	846.42	593.57	195.78	124.25	124.25
4	RMS	207.98	216.85	62.02	1.93	1.93
	Max	1228.31	1201.26	295.91	28.00	28.00

From the positioning results in Table 4. The first experiment located in the sub-urban environment was in the middle of two buildings. Where 3DMA GNSS RTK performs well in this location and obtains positioning RMS error within 10cm averagely. A relatively large position error can be found at the 3DMA BIE RTK for about 2m. This epoch error can also be found at other algorithms, such as 3DMA BIE@GT, which means this error could be caused by some unhealthy LOS satellite, like multipath, contributes to AR. The maximum positioning error is about 2m for proposed 3DMA BIE RTK, and this is identical to the theoretically the best result. However, for BIE without 3DMA, the maximum error can achieve over 10m, and BIE with higher elevation cutoff angle of 35 degrees is still about 9m.

Follows by experiment 2, it located in a deeper urban environment and surrounded by three buildings, and the mean value of skymask elevation angle is near 35-degree. This location should suffer from severe NLOS and multipath effect, however, RTK GNSS without the aid of 3DMA still capable of obtaining a good positioning result. This may be due to the multipath mitigation techniques in the sophisticated geodetic receiver. At this locaiton, the ambiguity dilution of precision (ADOP) and position dilution of precision (PDOP) without 3DMA exclusion are 0.05 and 2.01, respectively. Where the ADOP value is low here, as a result, able to obtain a good RTK positioning even without 3DMA, all algorithms perform well in this location, where RMS error is within 1cm. The RTK GNSS with higher elevation cut-off angle with 35 degrees slightly outperforms the others, and maximum positioning error is 1.97cm. It shows that a higher elevation cut-off angle can exclude those unhealthy satellites to improve the AR performance. 3DMA RTK GNSS can only exclude the NLOS satellite which assumed to be unhealthy, while cannot identify the multipath or diffraction satellite, and this can be an improvement in the future. In here, RTK GNSS without 3DMA can obtain a better positioning result compare to with 3DMA one. However, the positioning difference is in 0.01cm accuracy, and the standard deviation of the ground truth is 0.5cm. Therefore, we can only conclude that all algorithm obtains similar performance at this experiment but cannot fully provide the evidence on which algorithm outperforms others.

Unlike experiment 2 with an evenly distributed skymask elevation angle, experiment 3 and 4 are close to the building. Therefore, the skymask at these two locations are unevenly distributed. In other words, a higher elevation cutoff angle (BIE@EL35 solution) cannot improve the positioning results much compare with the proposed 3DMA GNSS RTK. And 3DMA GNSS RTK outperforms the RTK with elevation cutoff angle 35 degrees, and more than 20cm improvement on the RMS error can be found. These two experiments show that the proposed adaptive satellite exclusion scheme, which is using skymask for NLOS exclusion, is essential for urban GNSS RTK positioning.

As a reminder on experiment 3 result, the RMS error of 3DMA BIE RTK is 7.95cm while theoretically the best result, 3DMA BIE@GT, is 8.11cm. The difference in RMS error is within 1cm, while the uncertainty of ground truth is 1.33cm averagely with standard deviation is 0.77cm. As a result, we cannot conclude that the 3DMA BIE RTK is outperforming the theoretically the best result, but it can obtain similar or identical performance to it.

If we further look into the cumulative distribution function (CDF) of positioning error in Figure 4 (a) and (b) for experiment 1 and 4, respectively. Noted that here the positioning error only shows in centimeter-level, not all results are shown. From these results show that for RTK GNSS without the aid by 3D building model, the positioning results are worst. After increasing the cutoff elevation angle to 35 degrees (BIE@EL35 in Figure 4), the positioning performance can be increase slightly. About 80% of the position error is within 10cm. Finally, RKT GNSS can in an urban area be improved much with the aid of the 3D building model. For the 3DMA BIE RTK and theoretically the best result (3DMA BIE@GT), nearly all results can obtain a positioning error within 10cm. A larger improvement can be found in experiment 1 shown in Figure 4 (a), only about 60% of data is within 10cm error if no 3DMA. After

increasing the cutoff elevation angle, about 80% of error is within 10cm. While experiment 4 shown in Figure 4 (b), both RTK GNSS without 3DMA, nearly 80% of positioning error is within 10cm. These results show that the 3DMA GNSS RTK can improve the RTK positioning accuracy in the urban environment.

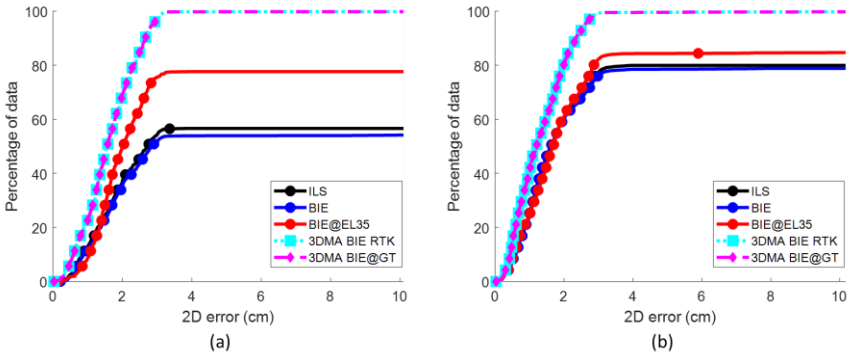

Figure 4 Cumulative distribution function (CDF) of positioning error on (a) experiment 1, (b) experiment 4, respectively. Noted that positioning error only shows the centimeter-level domain.

We selected heatmap of one epoch from experiment 4, shown in Figure 5(a). And the skymask at the same epoch on ground truth and accurate float position shown in Figure 5(b) and (c), respectively. Heatmap colour represents the mean-square-error (MSE) between the modelled and measured carrierphase measurements. And the darker blue represents, the better candidate is. In here, the conventional RTK GNSS (blue point) obtains about 1m of positioning error. And after distributing the candidates, the accurate float position (yellow point) locates about 80cm away from the ground truth. At the accurate float position, the LOS satellites are used for RTK GNSS again and result in a positioning error about 15cm. And this positioning result is the same as the theoretically the best solution, which RTK GNSS using the visibility at ground truth. And we look at the skymask at ground truth and accurate float position in Figure 5(b) and (c), respectively. The satellite visibility is identical at these two locations where only C27 is being excluded, while conventional RTK GNSS also using C27 for positioning. With exclusion on C27 can improve the RTK positioning from about 1m error to 15cm. These results show that although the visibility estimation position is far away from the ground truth, it can be still able to obtain an identical RTK solution to the truth visibility one.

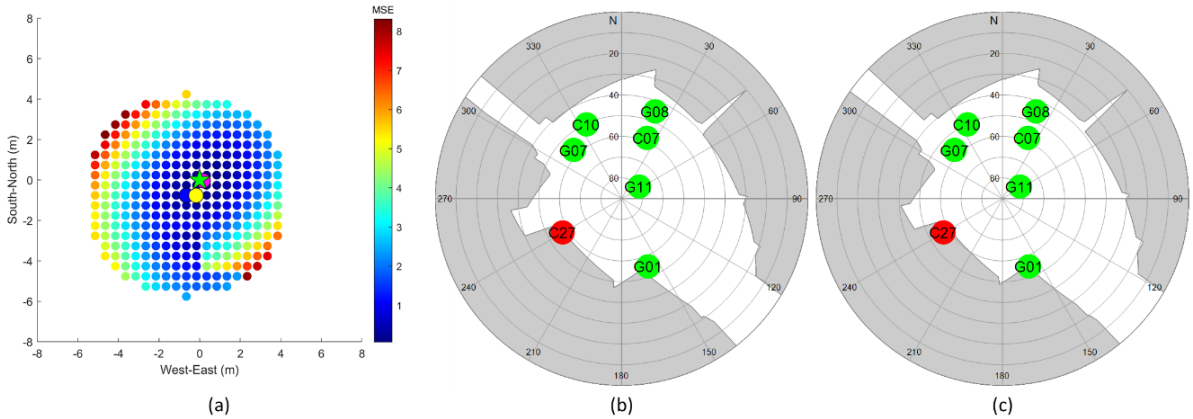

Figure 5 (a) Heatmap from experiment 4. Heatmap color is the mean-square-error (MSE) between the modelled and measured carrierphase measurements. The green star is the ground truth. Blue point is the conventional RTK GNSS solution, about 1m 2D error. Yellow point is the accurate float position for satellite visibility estimation, about 80cm 2D error. Purple point is the 3DMA GNSS RTK solution, about 18cm 2D error. (b) Skymask with satellite visibility at ground truth.7 (c) Skymask with satellite visibility at accurate float position. Green satellite means LOS satellite. Red satellite means NLOS satellite.

Geodetic-grade receiver has shown the 3DMA GNSS RTK can perform well in the urban area with 3DMA. Where proposed 3DMA BIE RTK performance is identical to the theoretically the best result, 3DMA BIE@GT, in all experiment. And the positioning RMS error is within 8cm in a different situation.

CONCLUSIONS AND FUTURE WORK

To conclude, this study proposes to bring the 3DMA GNSS concept integrates with the RTK for the urban environment application. The position hypothesis approach resolves the optimal satellite visibility to select the healthy measurements for the RTK solution. The results show that healthy satellite is important to AR and GNSS RTK solution. Exclusion dynamically with a 3D building model outperforms the performance of conventional RTK that exclude satellites that under a fixed elevation angle threshold. Cooperating the 3D building model to RTK GNSS in the urban area can improve the positioning results dramatically. From our designed experiment results, position accuracy in the urban area achieves within 10cm for the geodetic-grade receiver.

This study only shows the feasibility of 3DMA GNSS RTK with a static experiment by geodetic-grade receiver. Only NLOS satellite exclusion is presented in this study, but no multipath evaluation is implemented. In the near future, the multipath detection and exclusion scheme is required. Furthermore, the accurate float position by positioning hypothesis candidates is computationally intensive currently. The evaluation process may need to change to reduce the computation load, like incorporate the factor-graph-optimization (FGO) to resolve the best position iteratively for visibility estimation.

REFERENCES

[1] P. D. Groves, "Multipath vs. NLOS signals," *Inside GNSS*, vol. 8, pp. 40-42, 2013.

[2] L.-T. Hsu, "Analysis and modeling GPS NLOS effect in highly urbanized area," *GPS Solutions*, vol. 22, no. 1, p. 7, 2018.

[3] P. D. Groves, "It's Time for 3D Mapping–Aided GNSS," *Inside GNSS Magazine*, 09/01 2016.

[4] M. Obst, S. Bauer, and G. Wanielik, "Urban multipath detection and mitigation with dynamic 3D maps for reliable land vehicle localization," in *Proceedings of the 2012 IEEE/ION Position, Location and Navigation Symposium*, 23-26 April 2012 2012, pp. 685-691, doi: 10.1109/PLANS.2012.6236944.

[5] L.-T. Hsu, Y. Hu, and S. Kamijo, "3D building model-based pedestrian positioning method using GPS/GLONASS/QZSS and its reliability calculation," *GPS Solutions*, vol. 20, no. 3, pp. 413-428, 2016.

[6] S. Miura, L.-T. Hsu, and F. Chen, "GPS Error Correction With Pseudorange Evaluation Using Three-Dimensional Maps," *IEEE Transactions on Intelligent Transportation Systems*, vol. 16, no. 6, pp. 3104-3115, 2015.

[7] H.-F. Ng, G. Zhang, and L.-T. Hsu, "A Computation Effective Range-based 3D Mapping Aided GNSS with NLOS Correction Method," *Journal of Navigation*, pp. 1-21, 2020.

[8] H.-F. Ng, G. Zhang, and L.-T. Hsu, "GNSS NLOS Pseudorange Correction based on Skymask for Smartphone Applications," *Proceedings of the 32nd International Technical Meeting of the Satellite Division of The Institute of Navigation (ION GNSS+ 2019)*, pp. 109-119, 2019, doi: https://doi.org/10.33012/2019.17121.

[9] P. D. Groves, Q. Zhong, R. Faragher, and P. Esteves, "Combining Inertially-aided Extended Coherent Integration (Supercorrelation) with 3D-Mapping-Aided GNSS," *ION GNSS+ 2020*, 2020.

[10] R. B. Langley, "RTK GPS," *GPS World*, vol. 9, no. 9, pp. 70-76, 1998.

[11] P. J. G. Teunissen, "Least-Squares Estimation of the Integer GPS Ambiguities," *Invited lecture, section IV theory and methodology, IAG general meeting*, 1993.

[12] H. He, J. Li, Y. Yang, J. Xu, H. Guo, and A. Wang, "Performance assessment of single- and dual-frequency BeiDou/GPS single-epoch kinematic positioning," *GPS Solut*, vol. 18, no. 3, pp. 393-403, 2014, doi: 10.1007/s10291-013-0339-3.

[13] P. Teunissen, "On the computation of the best integer equivariant estimator," 2005.

[14] R. Odolinski and P. J. G. Teunissen, *On the Best Integer Equivariant Estimator for Low-cost Single-frequency Multi-GNSS RTK Positioning*. 2020, pp. 499-508.

[15] R. Odolinski and P. J. G. Teunissen, "Best integer equivariant estimation: performance analysis using real data collected by low-cost, single- and dual-frequency, multi-GNSS receivers for short- to long-baseline RTK positioning," *Journal of Geodesy*, vol. 94, no. 9, p. 91, 2020/09/02 2020, doi: 10.1007/s00190-020-01423-2.

[16] T. Takasu and A. Yasuda, "Cycle Slip Detection and Fixing by MEMS-IMU/GPS Integration for Mobile Environment RTK-GPS," in *Proceedings of the 21st International Technical Meeting of the Satellite Division of The Institute of Navigation (ION GNSS 2008)*, Savannah, GA, 01/01 2008, pp. 64-71.

[17] H. Tokura and N. Kubo, *Effective Satellite Selection Methods for RTK-GNSS NLOS Exclusion in Dense Urban Environments*. 2016, pp. 304-312.

[18] R. Furukawa, N. Kubo, and A. El-Mowafy, "Prediction of RTK-GNSS Performance in Urban Environments Using a 3D model and Continuous LoS Method," in *Proceedings of the 2020 International Technical Meeting of The Institute of Navigation*, San Diego, California, 2020, pp. 763-771.

[19] R. Furukawa, N. Kubo, and A. El-Mowafy, "Verification of GNSS Multipath and Positioning in Urban Areas Using 3D maps," *IEICE Communications Express*, vol. advpub, 2020, doi: 10.1587/comex.2020XBL0096.

[20] F. Zimmermann, C. Eling, L. Klingbeil, and H. Kuhlmann, "Precise Positioning of Uavs - Dealing with Challenging Rtk-Gps Measurement Conditions during Automated Uav Flights," *ISPRS Annals of Photogrammetry, Remote Sensing and Spatial Information Sciences*, vol. 42W3, p. 95, August 01, 2017 2017, doi: 10.5194/isprs-annals-IV-2-W3-95-2017.

[21] P. Jonge and C. C. J. M. Tiberius, "The LAMBDA method for integer ambiguity estimation: implementation aspects," *Delft Geodetic Computing Centre LGR Series*, vol. 12, 07/03 1998.

[22] G. Zhang, W. Wen, B. Xu, and L. Hsu, "Extending Shadow Matching to Tightly-Coupled GNSS/INS Integration System," *IEEE Transactions on Vehicular Technology*, vol. 69, no. 5, pp. 4979-4991, 2020, doi: 10.1109/TVT.2020.2981093.

[23] E. Realini and M. Reguzzoni, "Gogps: open source software for enhancing the accuracy of low-cost receivers by single-frequency relative kinematic positioning," *goGPS: open source software for enhancing the accuracy of low-cost receivers by single-frequency relative kinematic positioning*, vol. 24, no. 11, p. 115010, 2013, doi: 10.1088/0957-0233/24/11/115010.

[24] R. Odolinski, P. J. G. Teunissen, and D. Odijk, "Combined BDS, Galileo, QZSS and GPS single-frequency RTK," *GPS Solutions*, vol. 19, no. 1, pp. 151-163, 2015/01/01 2015, doi: 10.1007/s10291-014-0376-6.